Molecular basis of tactile specialization in the duck bill

Eve R. Schneider[a,1], Evan O. Anderson[a,1], Marco Mastrotto[a,b,c], Jon D. Matson[a], Vincent P. Schulz[d], Patrick G. Gallagher[d,e], Robert H. LaMotte[b,f], Elena O. Gracheva[a,b,c,2], and Sviatoslav N. Bagriantsev[a,2]

[a]Department of Cellular and Molecular Physiology, Yale University School of Medicine, New Haven, CT 06520; [b]Department of Neuroscience, Yale University School of Medicine, New Haven, CT 06520; [c]Program in Cellular Neuroscience, Neurodegeneration and Repair, Yale University School of Medicine, New Haven, CT 06520; [d]Department of Pediatrics, Yale University School of Medicine, New Haven, CT 06520; [e]Department of Genetics, Yale University School of Medicine, New Haven, CT 06520; and [f]Department of Anesthesiology, Yale University School of Medicine, New Haven, CT 06520

Edited by Joseph S. Takahashi, Howard Hughes Medical Institute, University of Texas Southwestern Medical Center, Dallas, TX, and approved October 10, 2017 (received for review May 26, 2017)

Tactile-foraging ducks are specialist birds known for their touch-dependent feeding behavior. They use dabbling, straining, and filtering to find edible matter in murky water, relying on the sense of touch in their bill. Here, we present the molecular characterization of embryonic duck bill, which we show contains a high density of mechanosensory corpuscles innervated by functional rapidly adapting trigeminal afferents. In contrast to chicken, a visually foraging bird, the majority of duck trigeminal neurons are mechanoreceptors that express the Piezo2 ion channel and produce slowly inactivating mechano-current before hatching. Furthermore, duck neurons have a significantly reduced mechano-activation threshold and elevated mechano-current amplitude. Cloning and electrophysiological characterization of duck Piezo2 in a heterologous expression system shows that duck Piezo2 is functionally similar to the mouse ortholog but with prolonged inactivation kinetics, particularly at positive potentials. Knockdown of Piezo2 in duck trigeminal neurons attenuates mechano current with intermediate and slow inactivation kinetics. This suggests that Piezo2 is capable of contributing to a larger range of mechano-activated currents in duck trigeminal ganglia than in mouse trigeminal ganglia. Our results provide insights into the molecular basis of mechanotransduction in a tactile-specialist vertebrate.

mechanosensitivity | mechanoreception | trigeminal ganglia | Piezo2 | mechano-gating

Of all of the sensory modalities possessed by vertebrates, mechanosensation remains the least understood at the cellular and molecular level. Rodents, the standard laboratory model for mechanosensation, mostly use whiskers for tactile discrimination, whereas other vertebrates rely on organs covered with glabrous (hairless) skin, such as fingertips and palms in primates, the star organ in the star-nosed mole, or the bill of tactile-foraging waterfowl (1–5). In the glabrous skin, many aspects of mechanical stimulation are sensed by Meissner and Pacinian corpuscles, the detectors of transient touch and vibration. The corpuscles are innervated by rapidly adapting neuronal mechanoreceptors, which function by a poorly understood molecular mechanism (6–8). With this in mind, we turned our attention to the domestic duck (*Anas platyrhynchos domesticus*), a tactile-specialist bird known for its sophisticated feeding behavior (9).

In contrast to visually foraging birds, such as chicken (*Gallus gallus domesticus*), ducks can find food in muddy water relying primarily on the sense of touch. In ducks and other tactile-foraging waterfowl, such as geese, the acquisition of tactile information is carried out by Herbst and Grandry corpuscles, the analogs of the mammalian Meissner and Pacinian corpuscles, respectively, which are located below the epidermis of the glabrous skin covering the bill, tongue, and oral cavity. In adult birds, the corpuscles are innervated by rapidly adapting mechanosensory afferents from trigeminal ganglia (TG) and relay tactile information from the periphery to the principal trigeminal nucleus (PrV) in the brainstem (1, 5, 10–12). In tactile foragers, the relative size of PrV is enlarged compared with visual foragers, suggesting the presence of an expanded population of mechanoreceptors in TG (13). Accordingly, we showed that the majority of neurons in TG of several species of tactile-foraging birds are large-diameter cells, consistent with the idea of mechanoreceptor expansion. We also demonstrated that duck TG neurons produce robust mechano-activated (MA) current in vitro (14).

In this study, we sought to investigate previously uncharacterized cellular and molecular adaptations for mechanoreception in the bill and trigeminal system of the domestic duck and to directly compare the mechanosensitivity of trigeminal neurons in tactile- and visually foraging birds. We also aimed to examine the molecular basis of the neuronal MA currents. Taking advantage of the fact that ducks are precocial birds, whose development largely completes *in ovo*, we focused on studying late-stage duck embryos, whose cells are also more amenable to experimental manipulations than those of adults. Here, we show that the embryonic duck bill contains mechanosensory corpuscles at a density comparable to that in the fingertips and palms of primates. Ex vivo electrophysiological experiments reveal that the molecular machinery that controls rapid adaptation of mechanically evoked firing is fully developed in the duck bill before hatching. We show the majority of neurons in duck, but not chicken, TG are low-threshold mechanoreceptors and that knockdown of the mechano-gated ion

Significance

Tactile-specialist birds of the Anatidae family possess unique mechanosensory abilities with which they efficiently select edible matter in muddy water without visual or olfactory cues. Mechanical stimuli are transmitted by trigeminal mechanoreceptors innervating the bill, a highly specialized tactile organ. We show mechanosensory specialization in ducks involves the formation of functional rapidly adapting mechanoreceptors prior to hatching. Unlike in visually foraging chicken, most trigeminal neurons in ducks are touch receptors, which develop following a unique pattern of neurotrophic factor receptor expression and produce robust mechano-current via the Piezo2 channel with novel properties. Our results uncover possible evolutionary adaptations contributing to potentiation of mechanoreception in an organ-specific manner and reveal the molecular identity of a neuronal mechanotransducer with prolonged inactivation kinetics.

Author contributions: E.R.S., E.O.A., E.O.G., and S.N.B. designed research; E.R.S., E.O.A., M.M., J.D.M., E.O.G., and S.N.B. performed research; E.R.S., E.O.A., V.P.S., P.G.G., R.H.L., E.O.G., and S.N.B. analyzed data; and E.R.S., E.O.A., P.G.G., R.H.L., E.O.G., and S.N.B. wrote the paper.

The authors declare no conflict of interest.

This article is a PNAS Direct Submission.

Data deposition: The sequence reported in this paper has been deposited in the GenBank database (accession no. KY012733).

See Commentary on page 12853.

[1]E.R.S. and E.O.A. contributed equally to this work.

[2]To whom correspondence may be addressed. Email: elena.gracheva@yale.edu or slav.bagriantsev@yale.edu.

This article contains supporting information online at www.pnas.org/lookup/suppl/doi:10.1073/pnas.1708793114/-/DCSupplemental.

channel Piezo2 suppresses intermediately and slowly inactivating mechano-current in these cells, contrasting with its role in mice as the mediator of only fast mechano-current. Our studies reveal a pattern of specialization in TG and uncover anatomical, neuronal, and molecular adaptations that subserve mechanoreception in a tactile-specialist vertebrate.

Results

Rapidly Adapting Mechanoreceptors in Duck Bill Are Functional Before Hatching. We performed histochemical analysis of the skin covering the dorsal bill of late-stage duck embryos (days E24–E26) using antibodies against the neuronal β-tubulin (Tuj1), also known to be expressed in the lamellar sheaths of Pacinian corpuscles (15). The staining revealed a network of nerve endings terminating in Herbst and Grandry corpuscles 100–500 μm below the surface of the skin (Fig. 1 *A*–*C* and Fig. S1). Using light-sheet and confocal microscopy combined with whole-mount immunostaining, we found the cumulative density of total corpuscles reaches 173 ± 6/mm^2 of dorsal bill skin (mean ± SD, n = 3) (Fig. 1*D* and Movie S1), rivaling the density in glabrous skin of other tactile specialists, such as in the fingertips of primates and the nose of the star-nosed mole (2, 5, 16, 17). Studies from adult ducks and geese showed that Grandry and Herbst corpuscles are innervated by trigeminal mechanoreceptors with rapidly adapting firing (10–12). These mechanoreceptors generate action potentials during the onset and offset of the mechanical stimulus but not during the static phase. Rapid adaptation stems from a poorly understood mechanism, which involves a contribution from the nerve afferent terminus and surrounding somatic components, such as the granular and lamellar cells in Grandry and Herbst corpuscles, respectively. To test if the mechanism of rapid adaptation is functional in embryonic corpuscles, we developed an ex vivo technique to extracellularly record electrical activity from the bodies of intact neurons in TG in response to mechanical stimulation of the bill (Fig. 1*E*). Remarkably, 10 of the 10 neurons that responded to a mechanical step indentation of the bill produced rapidly adapting discharges recorded in TG (Fig. 1 *F* and *G*). These data agree with the high density of mechanosensory corpuscles in the bill and demonstrate that the molecular machinery controlling rapid adaptation of mechanically evoked firing is fully developed before hatching. The accessibility of the duck embryos, rather than adult birds, to experimental manipulations allowed us to further explore the cellular and molecular basis of tactile specialization in duck TG.

Up-Regulation of Mechanoreceptors in TG of Tactile-Foraging Duck and Goose. Since afferent endings are essential for the development of mechanosensory corpuscles (3), the presence of an exceptionally dense corpuscle population in the duck bill strongly suggests the existence of a large number of mechanoreceptive neurons in TG. We previously demonstrated that TGs of several species of adult tactile-foraging birds from the *Anatidae* family mostly contain large-diameter cells, implying the presence of an unusually large population of mechanoreceptors (14). Here, we sought to directly test this hypothesis. First, we analyzed the expression of neurotrophic factor receptors TrkA and TrkB in TG of a tactile bird (duck) and a visually foraging bird (chicken). Along with other important factors, TrkA underlies the development of most nociceptors and thermoreceptors, and TrkB underlies the development of most mechanoreceptors (18). In mature ganglia of mice and rats, most somatosensory neurons express TrkA, whereas TrkB is limited to 10–30% of the cells (19–25). In the TG of a late-stage (E19–E20) domestic chicken embryo, a precocial visually foraging bird without tactile specialization in the beak, TrkA and TrkB were present in 36% and 27% of neurons, respectively, (Fig. 2 *A* and *B* and Fig. S2*A*), agreeing with data reported earlier (26). In striking contrast, we found that TrkA was expressed in only 7% of embryonic duck

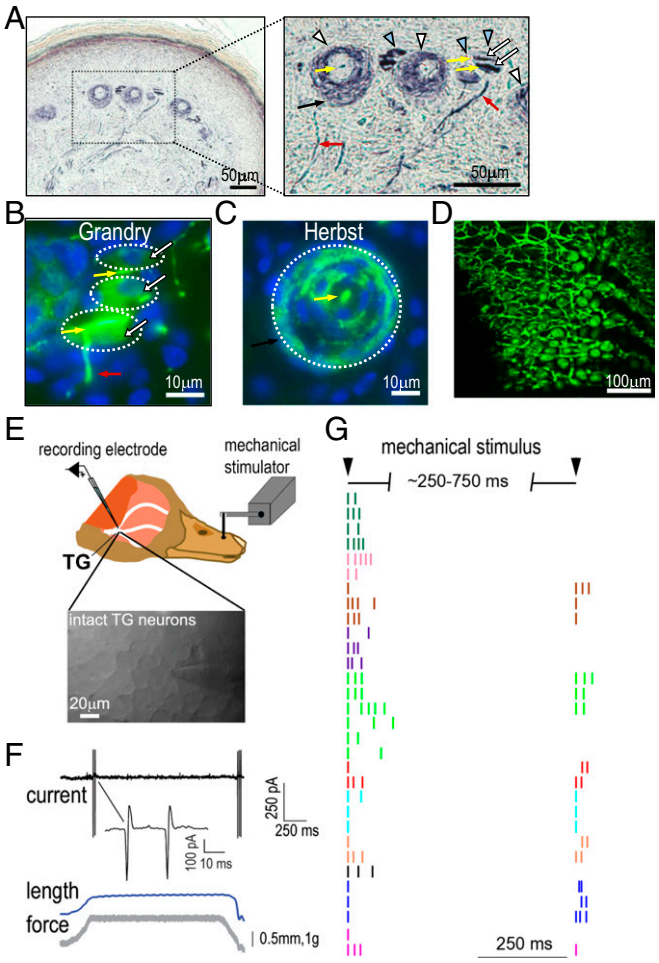

Fig. 1. Rapidly adapting mechanoreceptors in duck bill are functional before hatching. (*A*–*C*) Immunostaining of the skin from the lateral edge of the dorsal bill of a duck embryo with Tuj1 antibody reveals Herbst (white arrowhead) and Grandry (blue arrowhead) corpuscles innervated by trigeminal mechanoreceptors (red arrows). Mechanoreceptors terminate in the core of the corpuscles (yellow arrows), sandwiched between Tuj1-reactive satellite cells (white arrows; the cells are outlined with a dashed line in *B*) of Grandry corpuscles or surrounded by several layers of lamellar cells in Herbst corpuscles (the black arrow points at the outer layer of lamellar cells, indicated by a dashed line in *C*). Nuclear staining: DAPI. (*D*) Light-sheet microscopy and Tuj1 immunostaining of a whole-mount preparation of embryonic duck bill skin. Shown is a still image from Movie S1. (*E*) Ex vivo extracellular recordings from intact TG neurons in response to mechanical stimulation of the bill. (*Inset*) Exposed TG with an electrode attached to a neuron. (*F*) A representative rapidly adapting discharge recorded from a TG neuron in response to force- and indentation-controlled stimulation of the bill. (*G*) Raster plot demonstrates the prevalence of rapidly adapting mechanoreceptors among mechanosensitive duck TG neurons. Individual neurons are denoted by colors. Each tic mark indicates an action potential.

TG neurons, whereas the majority expressed TrkB (67%) (Fig. 2 *A* and *B* and Fig. S2*A*). Importantly, TrkA and TrkB were present in nearly identical proportions in TG neurons from late-embryonic and adult ducks (Fig. S2*B*), arguing against incomplete development as the cause for the observed neuronal distribution (27). These results show that, unlike other vertebrates such as mice or chickens, duck TG are predisposed to develop more mechanoreceptors than nociceptors and thermoreceptors. These data agree with the finding that TrkB is a critical factor for the normal development of mechanosensory corpuscles (28, 29).

Next, we analyzed the expression of the somatosensory ion channels TRPV1 and TRPM8, which together encompass most

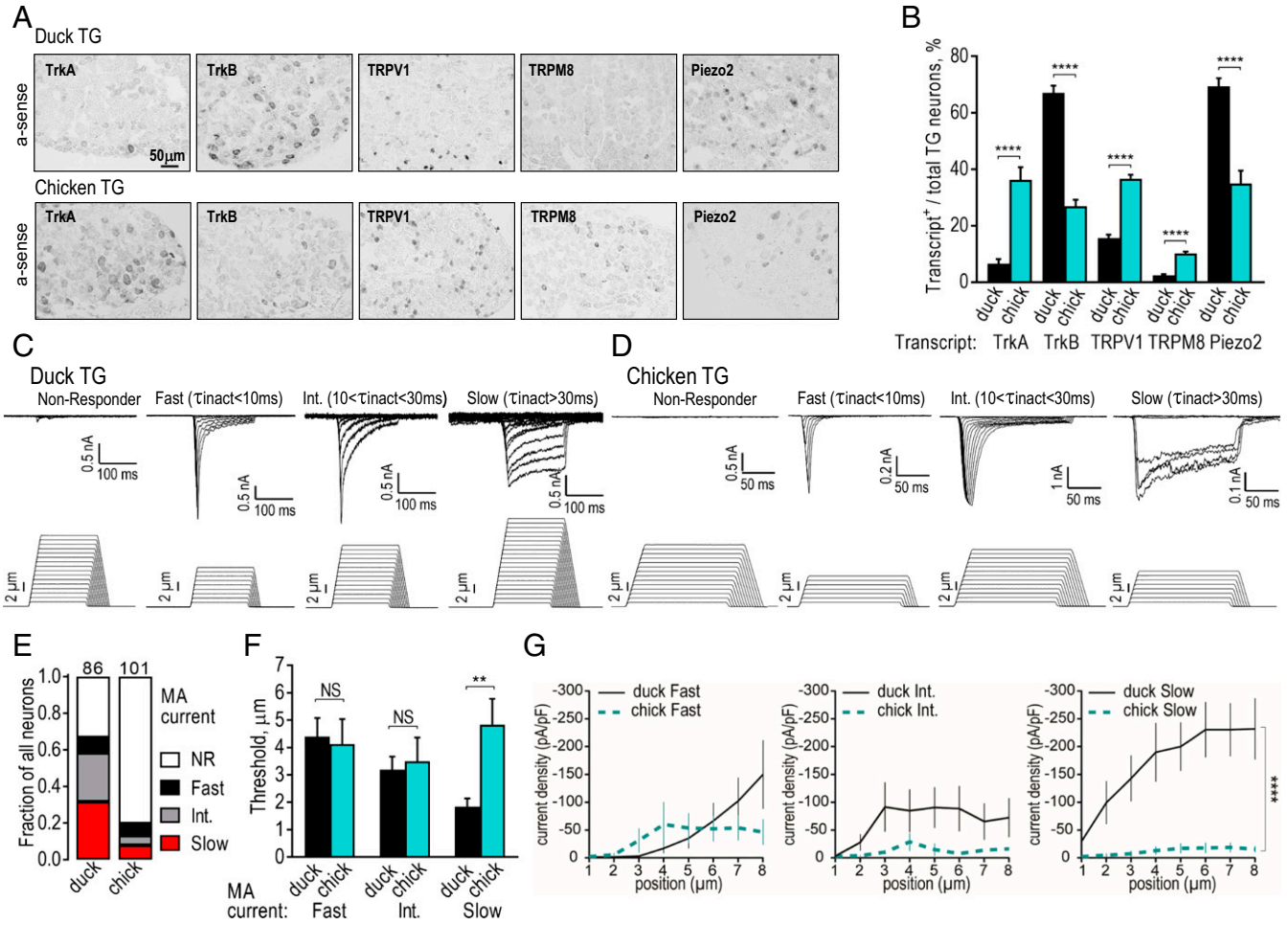

Fig. 2. Mechanoreceptor expansion is specific to duck TG. (*A*) Representative images of RNA in situ hybridization for the indicated targets in embryonic duck and chicken TG. (*B*) Quantification of the abundance of neurons expressing the indicated targets in duck and chicken TG (mean ± SE from ≥1,700 neurons obtained from at least seven TG sections from two or more animals for each target; $^{****}P \leq 0.0001$, two-tailed *t* test). (*C* and *D*) Exemplar whole-cell MA current traces recorded in dissociated TG neurons in the voltage-clamp mode at −74.6 mV holding potential in response to mechanical stimulation of the soma with a glass probe to the indicated depth. MA currents are classified based on the MA current inactivation rate (τ_{inact}). (*E*) Quantification of the prevalence of fast, intermediate, and slow MA current among mechanosensitive duck and chicken TG neurons. NR, nonresponder. (*F*) Quantification of the MA current activation threshold (mean ± SE) from 40 duck and 18 chicken neurons ($^{**}P \leq 0.01$, NS, not significant, $P > 0.05$; Kruskal–Wallis test with Dunn's multiple comparisons). (*G*) Peak MA current density measured at different indentation depths in mechanosensitive TG neurons (mean ± SE from 40 duck and 18 chicken neurons; $^{****}P \leq 0.0001$, ordinary two-way ANOVA with Bonferroni correction for multiple comparisons).

nociceptors and thermoreceptors (30, 31). In accordance with the paucity of TrkA$^+$ neurons, TRPV1 and TRPM8 were expressed in 16% and 2% of duck TG neurons, respectively. In contrast, the mechano-gated ion channel Piezo2 was present in 69% of cells (Fig. 2 *A* and *B* and Fig. S2*A*). On the other hand, in chicken TG TRPV1, TRPM8, and Piezo2 were present in 37%, 10%, and 35% of neurons, respectively (Fig. 2 *A* and *B* and Fig. S2*A*), a distribution similar to that found in mice (32–35). To investigate the prevalence of mechanoreceptors in other tactile-foraging species, we analyzed TG from the Canada goose (*Branta canadensis*), a precocial tactile-foraging bird from the *Anserinae* subfamily (10). In adult goose, the majority of TG neurons expressed Piezo2 (53%), and far fewer expressed TRPV1 (20%) and TRPM8 (4%), a distribution similar to that in duck TG (Fig. S3). Taken together, our histological analyses suggest that mechanoreceptor expansion in TG is not a general avian feature but may be specific to tactile-foraging ducks and geese.

To complement our histological analysis, we investigated the mechanosensitivity of duck and chicken TG neurons directly by recording MA current in response to a stimulation of the cellular soma with a glass probe. Based on the rate of exponential decay, MA currents are classified as fast, intermediately, and slowly inactivating (14, 36–39). The three types of current were present in neurons from both species (Fig. 2 *C* and *D*). However, whereas 57 of 86 (66%) duck TG neurons produced MA current in response to mechanical stimulation, only 20 of 101 (20%) chicken neurons were mechanosensitive (Fig. 2*E*). In comparison with chicken, duck neurons had a significantly reduced mechano-activation threshold and elevated MA current density in cells with slow MA current (Fig. 2 *F* and *G*). Thus, not only are mechanosensitive neurons more numerous in duck than in chicken TG, but neurons with slow MA current exhibit an elevated ability to convert touch into excitation.

It is interesting that neurons with fast MA current are the least numerous group in ducks (12% of all mechanosensitive cells) and are the most numerous group in chicken (44%) (Fig. 2*E*). The distribution of MA current types among chicken neurons is similar to that found in mice and rats, where fast MA current is present in 30–60% of mechanosensitive neurons (14, 27, 34, 40). The prevalence of neurons with slow inactivation kinetics in ducks (47%) together with a low threshold of activation and high MA current density could reflect somatosensory specialization

toward the detection of light touch via increased charge influx upon mechanical stimulation. Taken together, our histological and functional data show an up-regulation of the mechanoreceptor population in duck TG, consistent with the pattern of TrkB and TrkA expression. The expansion of mechanoreceptors in duck TG reveals a pattern of somatosensory ganglia specialization sufficient to innervate the exceptionally dense population of Grandry and Herbst corpuscles in duckbill skin.

Piezo2 Mediates a Subset of Mechano-Current with Prolonged Inactivation in Duck TG. We sought to investigate the molecular basis of touch detection in duck neuronal mechanoreceptors, taking advantage of our finding that this is the most abundant neuronal group in duck TG. MA current is essential for neuronal touch sensitivity. Piezo2 is known to contribute exclusively to the generation of fast MA current in mouse somatosensory neurons (34, 35, 41–43), whereas MA currents with intermediate and slow inactivation kinetics are thought to be Piezo2-independent (44–46). Since the percentage of duck neurons expressing Piezo2 far exceeds the percentage of neurons with fast MA current, which are the least numerous group of mechanosensitive neurons in duck TG, we hypothesized that Piezo2 also contributes to the MA currents with prolonged inactivation. To test this, we first cloned Piezo2 from duck TG and analyzed its functional properties in HEK293T cells in comparison with mouse Piezo2 (mPiezo2), a well-characterized ortholog. Immunoblot showed that duck Piezo2 protein (dPiezo2) is expressed in transfected HEK293T cells in duck TG and bill skin (Fig. 3*A* and Fig. S4). dPiezo2 produced nonselective, Gd^{3+}-sensitive MA current with an activation threshold identical to the mouse ortholog, mPiezo2 (Fig. 3 *B*, *C*, *F*, and *G*). The similarly high amplitude of mouse and dPiezo2 MA current (Fig. 3*D*) eliminates the potentially confounding effect of endogenous Piezo1 in these cells (44). dPiezo2 demonstrated significantly slower inactivation kinetics than mPiezo2 at −80 mV (mPiezo2 τ_{inact} = 3.1 ± 0.17 ms, dPiezo2 τ_{inact} = 5.1 ± 0.47 ms, mean ± SE, n = 26–29) (Fig. 3*E*). This difference becomes larger at depolarized potentials, where the rate of dPiezo2 inactivation converts from fast to slow (τ_{inact} >30 ms) (Fig. 3 *G* and *H*). Although the increase in inactivation rate is small at physiologically relevant voltages, these data show that the inactivation rate of dPiezo2 can be reversibly converted from fast to slow in the same cell.

To test the role of Piezo2 in the generation of MA current in duck TG neurons, we used fluorescently labeled siRNA designed against a region in Piezo2 previously reported to be susceptible to siRNA-mediated knockdown (34, 41). Treatment of dissociated TG neurons with siRNA against Piezo2 decreased Piezo2 mRNA and protein by ∼40%, while no decrease was detected in control (Fig. 4 *A*–*C*). siRNA treatment had no noticeable effect on neuronal fitness, as revealed by unchanged input resistance, resting membrane potential, and cell capacitance in fluorescent siRNA-containing neurons (Fig. S5). At the same time, the down-regulation of Piezo2 was accompanied by an ∼50% increase in the fraction of neurons without MA current (Fig. 4*D*). These additional mechanoinsensitive neurons are probably those in which Piezo2 was the major mechanotransducer and in which expression knockdown was the most efficient. Notably, while Piezo2 knockdown did not change the apparent threshold of mechanical activation (Fig. S6), it led to a significant decrease in MA current density in neurons with intermediate and slow MA current (Fig. 4 *E* and *F*). The remaining MA current in these cells could be due to the presence of other mechanotransducers in addition to Piezo2 or to incomplete knockdown. Taken together, our data reveal that Piezo2 contributes to the generation of intermediate and slow MA current in duck trigeminal neurons.

Discussion

Feeding in ducks relies on the precise acquisition of tactile information from transient touch and vibration. Rapidly adapting mechanoreceptors are ideal for encoding the fast-acting stimuli

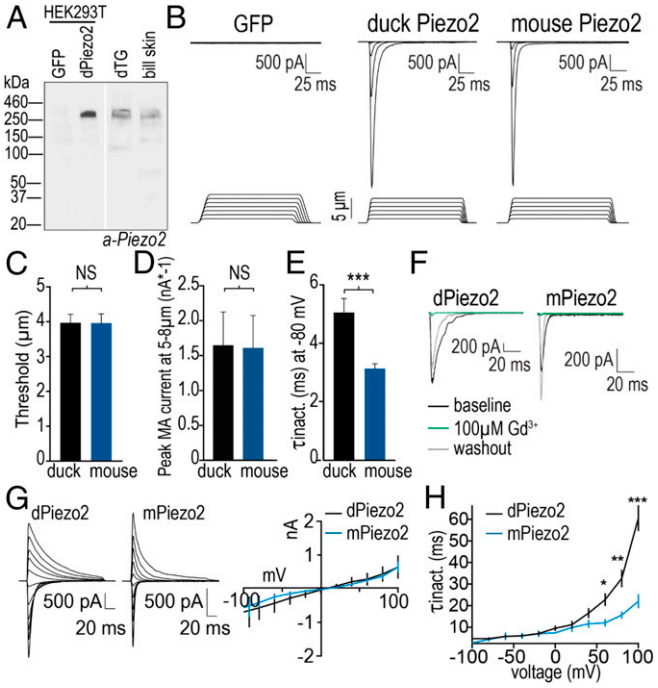

Fig. 3. dPiezo2 has slower kinetics of inactivation than the mouse channel. (*A*) Western blot shows Piezo2 expression in duck TG (dTG), bill skin, and HEK293T cells transfected with dPiezo2. (*B*) Representative whole-cell MA current traces recorded in the voltage-clamp mode (V_{hold} −80 mV) in HEK293T cells expressing the indicated constructs, in response to mechanical stimulation of the cellular soma with a glass probe. (*C*–*E*) Quantification of the Piezo2 MA current activation threshold (*C*), amplitude (*D*), and inactivation rate τ_{inact} (*E*) in HEK293T cells at −80 mV (data are the mean ± SE from 29 dPiezo2- and 26 mPiezo2-expressing cells). Tau values averaged across traces with −0.1 to −2 nA MA current; ***$P \leq 0.001$; NS, not significant (Welch's t test). (*F*) Exemplar MA current traces showing reversible inhibition of dPiezo2 MA current by Gd^{3+} in HEK293T cells (V_{hold} −80 mV). (*G*) Representative traces and current–voltage plots of Piezo2 MA currents in HEK293T cells evoked at different voltages in response to a mechanical indentation of 6–8 µm (mean ± SE, n = 2–6 for each voltage). (*H*) Quantification of MA current inactivation from *E* (mean ± SE, *$P \leq 0.05$, **$P \leq 0.01$, ***$P \leq 0.001$, two-way ANOVA with Bonferroni-corrected paired comparisons; n = 2–6 for each voltage).

because they fire only during the dynamic phase of the stimulus, providing high temporal resolution. Here we show that the mechanism that produces the rapid adaptation of afferent firing is fully developed *in ovo*, providing insight on the observation that ducklings can forage side-by-side with adults shortly after hatching.

Consistent with the high density of the corpuscles in the bill skin, our histological and electrophysiological data show that the majority of duck trigeminal neurons are mechanoreceptors. The expansion of mechanoreceptors is unusual for somatosensory ganglia of rats and mice, where most neurons are nociceptors and thermoreceptors (32). Studies in rodents and chickens showed that while $TrkB^+$ mechanoreceptors arise as the dominant group early in development, they are later outnumbered by $TrkA^+$ nociceptors and thermoreceptors (18, 27). We find that the majority of late-embryonic and adult duck TG neurons express TrkB, whereas TrkA expression is limited to a small population of cells. This suggests that mechanoreceptor expansion in tactile-foraging ducks is driven by a developmental program different from that found in chicken, a visual forager, or in rodents.

Neuronal mechanoreceptors are essential for touch physiology. Even though the somatic components of the mechanosensory end-organs play important roles in detecting physical stimuli, the neurons are innately mechanosensitive, i.e., they can covert touch into excitatory MA current in the absence of other tissue

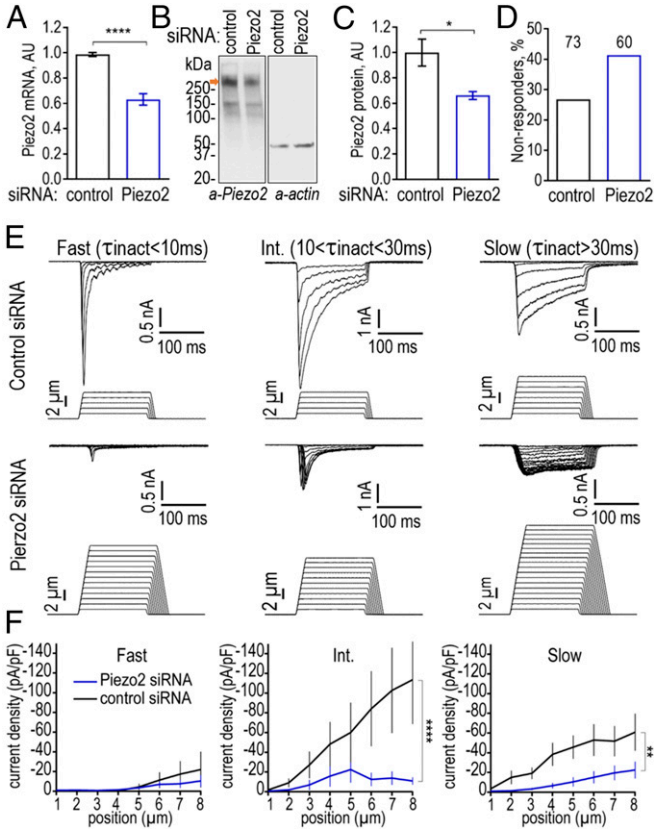

Fig. 4. Knockdown of Piezo2 suppresses intermediate and slow mechano-current in duck TG. (*A*) Quantification of siRNA-mediated Piezo2 mRNA knock-down in dissociated duck TG neurons relative to untreated cells by qPCR (mean ± SE from six independent transfections; $^{****}P \leq 0.0001$, two-tailed *t* test). (*B* and *C*) Immunoblot analysis (*B*) and quantification (*C*) of the knockdown of Piezo2 protein expression (red arrow) in dissociated duck TG after control or Piezo2 siRNA treatment, normalized to actin in each sample (mean ± SE from 12 transfections from three independent TG preparations; $^{*}P \leq 0.05$, two-tailed *t* test). (*D*) Quantification of the proportion of mechano-insensitive TG neurons after control or Piezo2 siRNA treatment. Recordings were made only from neurons that received siRNA, as determined by fluorescence. (*E* and *F*) Exemplar whole-cell MA current traces (*E*) and quantification of MA current density (*F*) in dissociated TG neurons after control or Piezo2 siRNA treatment (mean ± SE, $^{****}P \leq 0.0001$, $^{**}P \leq 0.005$, ordinary two-way ANOVA with Bonferroni correction for multiple comparisons). Fast MA current: $n = 4$ control siRNA, $n = 5$ Piezo2 siRNA; intermediate (Int.) MA current: $n = 15$ control siRNA, $n = 9$ Piezo2 siRNA; slow MA current: $n = 31$ control siRNA, $n = 21$ Piezo2 siRNA. E_{hold}, −74.6 mV.

components (47). Mechanical stimulation evokes three major types of MA current in somatosensory neurons: fast, intermediately, and slowly inactivating (14, 36–39). In mouse somatosensory neurons, Piezo2 depletion by siRNA (34, 41) or via conditional knockout (35, 42) eliminates only fast MA current, suggesting that the other MA current types are Piezo2-independent. We show that neurons with fast MA current represent the smallest group of mechanosensitive cells in duck TG, whereas many more neurons express MA current with prolonged inactivation. Knockdown of Piezo2 expression by siRNA significantly suppresses intermediate and slow MA current density, suggesting that Piezo2 contributes to the generation of these types of current. We did not detect an effect of Piezo2 knockdown on fast MA current, possibly due to the very low abundance of this group of neurons. Our results do not rule out the existence of other mechanotransducers with slow or intermediate inactivation kinetics, which may or may not coexpress with Piezo2 in the same neuron. The contribution of such mechanotransducers could be more prominent in mouse neurons than in duck cells, explaining the absence of an effect of Piezo2 knockdown on these MA currents. Overall, our results show that Piezo2 is an evolutionarily conserved mediator of neuronal mechanosensation in vertebrates and that the channel can contribute to more than one type of MA current in somatosensory neurons.

The rate of Piezo2 inactivation controls the amount of excitatory charge entering the cell upon mechanical stimulation. Inactivation of Piezo2 and its homolog Piezo1 can be prolonged at positive potentials (34, 48), by mutations (49–55), pharmacologically (56, 57), or by the destruction of the cytoskeleton or after repeated stimulation (58), fluid shear stress (59), or osmotic swelling (60). These data establish that Piezo channel kinetics is modulated by intracellular factors. Interestingly, single-channel recordings from Piezo1 in a lipid bilayer revealed the absence of inactivation (61), suggesting that Piezo channels could be intrinsically non- or slowly inactivating even at potentials close to physiological, whereas the fast inactivation observed in cells requires additional components. We therefore hypothesize that the differences in dPiezo2 kinetics of inactivation in HEK293T cells and duck TG neurons are due to posttranslational modifications, properties of the plasma membrane, cytoskeleton, auxiliary subunits, or gating modifiers (57, 60, 62–66), which are present (or absent) in such neurons and remain to be identified.

It remains to be determined which type of MA current is present in the rapidly adapting mechanoreceptors that innervate Grandry and Herbst corpuscles. Studies in cat Pacinian corpuscles showed that mechanical stimulation of the inner core triggers slowly inactivating receptor potential, indicating the presence of a mechanotransducer with slowly inactivating MA current (67). It is therefore possible that the mechanoreceptors with rapidly adapting firing that innervate the vibration-sensitive Herbst or Pacinian corpuscles express slowly inactivating MA current, which, as we show, is partially mediated by Piezo2. Consistently, Piezo2 mutants with prolonged inactivation transduce high-frequency stimulation much more efficiently than the fast-inactivating wild-type channel (68). The importance of Piezo2 for rapidly adapting mechanoreceptors could be general: a recent report documented that humans without functional Piezo2 exhibit deficits in the perception of vibratory stimuli in their hairless skin in the frequency range detectable by Pacinian corpuscles (69).

The high density of Grandry and Herbst corpuscles in the bill together with the expansion of mechanoreceptors in TG suggest duck embryos as a potential model to study functional properties and molecular organization of rapidly adapting mechanoreceptors innervating glabrous skin. Genome editing-based approaches and cell type-specific control of activation in duck cells will be needed to reveal other mechanotransducers and to delineate the contribution of somatic and neuronal components to the fine-tuning of the mechanosensory corpuscles.

Materials and Methods

Animal procedures were approved by and performed in compliance with the Institutional Animal Care and Use Committee of Yale University. Immunohistochemistry, biochemical analysis, microscopy, cloning, and in situ hybridization were performed using standard procedures. For detailed description of ex vivo and patch-clamp electrophysiology, see *SI Materials and Methods*.

ACKNOWLEDGMENTS. We thank members of the E.O.G. and S.N.B. laboratories for comments on the study, Sue Ann Mentone for immunohistochemistry, Chao Ma for advice on ex vivo recordings, Kara Marshall and Ellen Lumpkin for advice on whole-mount histology, Uwe Schröer for lending equipment for light-sheet microscopy, Ardem Patapoutian for the gift of plasmid, and Jeffrey Laursen and Charles Pederson for goose tissues. E.R.S. was supported by NIH Training Grant T32HD007094 (to P.G.G.) and a Postdoctoral Fellowship from the Arnold and Mabel Beckman Foundation. E.O.A. is an Edward L. Tatum Fellow and was supported by the Gruber Foundation. This work was funded by NIH National Institute of Diabetes and Digestive and Kidney Diseases Grant R01DK104046 (to P.G.G.), by fellowships from the Arnold and Mabel Beckman Foundation and Rita Allen Foundation, by NIH National Institute of Neurological Disorders and Stroke (NINDS) Grant 1R01NS091300-01A1 (to E.O.G.), and by National Science Foundation Career Award 1453167 and NIH NINDS Grant 1R01NS097547-01A1 (to S.N.B.).

1. Berkhoudt H (1980) The morphology and distribution of cutaneous mechanoreceptors (Herbst and Grandry corpuscles) in bill and tongue of the mallard (Anas platyrhynchos L.). *Neth J Zool* 30:1–34.
2. Catania KC (2011) The sense of touch in the star-nosed mole: From mechanoreceptors to the brain. *Philos Trans R Soc Lond B Biol Sci* 366:3016–3025.
3. Vega JA, García-Suárez O, Montaño JA, Pardo B, Cobo JM (2009) The Meissner and Pacinian sensory corpuscles revisited new data from the last decade. *Microsc Res Tech* 72:299–309.
4. Gerhold KA, et al. (2013) The star-nosed mole reveals clues to the molecular basis of mammalian touch. *PLoS One* 8:e55001.
5. Schneider ER, Gracheva EO, Bagriantsev SN (2016) Evolutionary specialization of tactile perception in vertebrates. *Physiology (Bethesda)* 31:193–200.
6. Abraira VE, Ginty DD (2013) The sensory neurons of touch. *Neuron* 79:618–639.
7. Fleming MS, Luo W (2013) The anatomy, function, and development of mammalian Aβ low-threshold mechanoreceptors. *Front Biol (Beijing)* 8:408–420.
8. Hao J, Bonnet C, Amsalem M, Ruel J, Delmas P (2015) Transduction and encoding sensory information by skin mechanoreceptors. *Pflugers Arch* 467:109–119.
9. Zweers GA, Gerritsen AFC, Kranenburg-Voogd PJv (1977) *Mechanics of Feeding of the Mallard (Anas Platyrhynchos, L.; Aves, Anseriformes): The Lingual Apparatus and the Suction-Pressure Pump Mechanism of Straining* (S. Karger AG, Basel, Switzerland).
10. Gottschaldt K-M (1974) The physiological basis of tactile sensibility in the beak of geese. *J Comp Physiol* 95:29–47.
11. Leitner LM, Roumy M (1974) Mechanosensitive units in the upper bill and in the tongue of the domestic duck. *Pflugers Arch* 346:141–150.
12. Gregory JE (1973) An electrophysiological investigation of the receptor apparatus of the duck's bill. *J Physiol* 229:151–164.
13. Gutiérrez-Ibáñez C, Iwaniuk AN, Wylie DR (2009) The independent evolution of the enlargement of the principal sensory nucleus of the trigeminal nerve in three different groups of birds. *Brain Behav Evol* 74:280–294.
14. Schneider ER, et al. (2014) Neuronal mechanism for acute mechanosensitivity in tactile-foraging waterfowl. *Proc Natl Acad Sci USA* 111:14941–14946.
15. Pawson L, Slepecky NB, Bolanowski SJ (2000) Immunocytochemical identification of proteins within the Pacinian corpuscle. *Somatosens Mot Res* 17:159–170.
16. Sawyer EK, Catania KC (2016) Somatosensory organ topography across the star of the star-nosed mole (Condylura cristata). *J Comp Neurol* 524:917–929.
17. Verendeev A, et al. (2015) Comparative analysis of Meissner's corpuscles in the fingertips of primates. *J Anat* 227:72–80.
18. Lallemend F, Ernfors P (2012) Molecular interactions underlying the specification of sensory neurons. *Trends Neurosci* 35:373–381.
19. Kobayashi K, et al. (2005) Distinct expression of TRPM8, TRPA1, and TRPV1 mRNAs in rat primary afferent neurons with adelta/c-fibers and colocalization with trk receptors. *J Comp Neurol* 493:596–606.
20. Mu X, Silos-Santiago I, Carroll SL, Snider WD (1993) Neurotrophin receptor genes are expressed in distinct patterns in developing dorsal root ganglia. *J Neurosci* 13:4029–4041.
21. Huang EJ, et al. (1999) Expression of Trk receptors in the developing mouse trigeminal ganglion: In vivo evidence for NT-3 activation of TrkA and TrkB in addition to TrkC. *Development* 126:2191–2203.
22. Li L, et al. (2011) The functional organization of cutaneous low-threshold mechanosensory neurons. *Cell* 147:1615–1627.
23. Ma Q, Fode C, Guillemot F, Anderson DJ (1999) Neurogenin1 and neurogenin2 control two distinct waves of neurogenesis in developing dorsal root ganglia. *Genes Dev* 13:1717–1728.
24. Luo W, Enomoto H, Rice FL, Milbrandt J, Ginty DD (2009) Molecular identification of rapidly adapting mechanoreceptors and their developmental dependence on ret signaling. *Neuron* 64:841–856.
25. Hallbook F, et al. (1995) Neurotrophins and their receptors in chicken neuronal development. *Int J Dev Biol* 39:855–868.
26. Williams R, Bäckström A, Kullander K, Hallböök F, Ebendal T (1995) Developmentally regulated expression of mRNA for neurotrophin high-affinity (trk) receptors within chick trigeminal sensory neurons. *Eur J Neurosci* 7:116–128.
27. Lechner SG, Frenzel H, Wang R, Lewin GR (2009) Developmental waves of mechanosensitivity acquisition in sensory neuron subtypes during embryonic development. *EMBO J* 28:1479–1491.
28. González-Martínez T, et al. (2004) Absence of Meissner corpuscles in the digital pads of mice lacking functional TrkB. *Brain Res* 1002:120–128.
29. de Carlos F, et al. (2006) Abnormal development of pacinian corpuscles in double trkB;trkC knockout mice. *Neurosci Lett* 410:157–161.
30. Knowlton WM, et al. (2013) A sensory-labeled line for cold: TRPM8-expressing sensory neurons define the cellular basis for cold, cold pain, and cooling-mediated analgesia. *J Neurosci* 33:2837–2848.
31. Mishra SK, Tisel SM, Orestes P, Bhangoo SK, Hoon MA (2011) TRPV1-lineage neurons are required for thermal sensation. *EMBO J* 30:582–593.
32. Le Pichon CE, Chesler AT (2014) The functional and anatomical dissection of somatosensory subpopulations using mouse genetics. *Front Neuroanat* 8:21.
33. Bron R, Wood RJ, Brock JA, Ivanusic JJ (2014) Piezo2 expression in corneal afferent neurons. *J Comp Neurol* 522:2967–2979.
34. Coste B, et al. (2010) Piezo1 and Piezo2 are essential components of distinct mechanically activated cation channels. *Science* 330:55–60.
35. Ranade SS, et al. (2014) Piezo2 is the major transducer of mechanical forces for touch sensation in mice. *Nature* 516:121–125.
36. Hu J, Lewin GR (2006) Mechanosensitive currents in the neurites of cultured mouse sensory neurones. *J Physiol* 577:815–828.
37. Coste B, Crest M, Delmas P (2007) Pharmacological dissection and distribution of NaN/Nav1.9, T-type Ca2+ currents, and mechanically activated cation currents in different populations of DRG neurons. *J Gen Physiol* 129:57–77.
38. Hao J, Delmas P (2010) Multiple desensitization mechanisms of mechanotransducer channels shape firing of mechanosensory neurons. *J Neurosci* 30:13384–13395.
39. Rugiero F, Drew LJ, Wood JN (2010) Kinetic properties of mechanically activated currents in spinal sensory neurons. *J Physiol* 588:301–314.
40. Viatchenko-Karpinski V, Gu JG (2016) Mechanical sensitivity and electrophysiological properties of acutely dissociated dorsal root ganglion neurons of rats. *Neurosci Lett* 634:70–75.
41. Lou S, Duan B, Vong L, Lowell BB, Ma Q (2013) Runx1 controls terminal morphology and mechanosensitivity of VGLUT3-expressing C-mechanoreceptors. *J Neurosci* 33:870–882.
42. Woo SH, et al. (2015) Piezo2 is the principal mechanotransduction channel for proprioception. *Nat Neurosci* 18:1756–1762.
43. Anderson EO, Schneider ER, Bagriantsev SN (2017) Piezo2 in cutaneous and proprioceptive mechanotransduction in vertebrates. *Curr Top Membr* 79:197–217.
44. Dubin AE, et al. (2017) Endogenous Piezo1 can confound mechanically activated channel identification and characterization. *Neuron* 94:266–270.
45. Hong GS, Lee B, Oh U (2017) Evidence for mechanosensitive channel activity of tentonin 3/TMEM150C. *Neuron* 94:271–273.e2.
46. Hong GS, et al. (2016) Tentonin 3/TMEM150c confers distinct mechanosensitive currents in dorsal-root ganglion neurons with proprioceptive function. *Neuron* 91:708–710.
47. McCarter GC, Reichling DB, Levine JD (1999) Mechanical transduction by rat dorsal root ganglion neurons in vitro. *Neurosci Lett* 273:179–182.
48. Gnanasambandam R, Bae C, Gottlieb PA, Sachs F (2015) Ionic selectivity and permeation properties of human PIEZO1 channels. *PLoS One* 10:e0125503.
49. Coste B, et al. (2013) Gain-of-function mutations in the mechanically activated ion channel PIEZO2 cause a subtype of distal arthrogryposis. *Proc Natl Acad Sci USA* 110:4667–4672.
50. Bae C, Gnanasambandam R, Nicolai C, Sachs F, Gottlieb PA (2013) Xerocytosis is caused by mutations that alter the kinetics of the mechanosensitive channel PIEZO1. *Proc Natl Acad Sci USA* 110:E1162–E1168.
51. Bae C, Gottlieb PA, Sachs F (2013) Human PIEZO1: Removing inactivation. *Biophys J* 105:880–886.
52. Bae C, Suchyna TM, Ziegler L, Sachs F, Gottlieb PA (2016) Human PIEZO1 ion channel functions as a split protein. *PLoS One* 11:e0151289.
53. Albuisson J, et al. (2013) Dehydrated hereditary stomatocytosis linked to gain-of-function mutations in mechanically activated PIEZO1 ion channels. *Nat Commun* 4:1884.
54. Coste B, et al. (2015) Piezo1 ion channel pore properties are dictated by C-terminal region. *Nat Commun* 6:7223.
55. Glogowska E, et al. (July 17, 2017) Novel mechanisms of PIEZO1 dysfunction in hereditary xerocytosis. *Blood*, 10.1182/blood-2017-05-786004.
56. Syeda R, et al. (2015) Chemical activation of the mechanotransduction channel Piezo1. *Elife* 4:e07369.
57. Dubin AE, et al. (2012) Inflammatory signals enhance piezo2-mediated mechanosensitive currents. *Cell Rep* 2:511–517.
58. Gottlieb PA, Bae C, Sachs F (2012) Gating the mechanical channel Piezo1: A comparison between whole-cell and patch recording. *Channels (Austin)* 6:282–289.
59. Ranade SS, et al. (2014) Piezo1, a mechanically activated ion channel, is required for vascular development in mice. *Proc Natl Acad Sci USA* 111:10347–10352.
60. Jia Z, Ikeda R, Ling J, Viatchenko-Karpinski V, Gu JG (2016) Regulation of Piezo2 mechanotransduction by static plasma membrane tension in primary afferent neurons. *J Biol Chem* 291:9087–9104.
61. Syeda R, et al. (2016) Piezo1 channels are inherently mechanosensitive. *Cell Rep* 17:1739–1746.
62. Borbiro I, Badheka D, Rohacs T (2015) Activation of TRPV1 channels inhibits mechanosensitive Piezo channel activity by depleting membrane phosphoinositides. *Sci Signal* 8:ra15.
63. Poole K, Herget R, Lapatsina L, Ngo HD, Lewin GR (2014) Tuning piezo ion channels to detect molecular-scale movements relevant for fine touch. *Nat Commun* 5:3520.
64. Morley SJ, et al. (2016) Acetylated tubulin is essential for touch sensation in mice. *Elife* 5:e20813.
65. Lewis AH, Grandl J (2015) Mechanical sensitivity of Piezo1 ion channels can be tuned by cellular membrane tension. *Elife* 4:e12088.
66. Qi Y, et al. (2015) Membrane stiffening by STOML3 facilitates mechanosensation in sensory neurons. *Nat Commun* 6:8512.
67. Mendelson M, Lowenstein WR (1964) Mechanisms of receptor adaptation. *Science* 144:554–555.
68. Lewis AH, Cui AF, McDonald MF, Grandl J (2017) Transduction of repetitive mechanical stimuli by Piezo1 and Piezo2 ion channels. *Cell Rep* 19:2572–2585.
69. Chesler AT, et al. (2016) The role of PIEZO2 in human mechanosensation. *N Engl J Med* 375:1355–1364.
70. Moreton J, Dunham SP, Emes RD (2014) A consensus approach to vertebrate de novo transcriptome assembly from RNA-seq data: Assembly of the duck (Anas platyrhynchos) transcriptome. *Front Genet* 5:190.
71. Ma C, Donnelly DF, LaMotte RH (2010) In vivo visualization and functional characterization of primary somatic neurons. *J Neurosci Methods* 191:60–65.

Supporting Information

Schneider et al. 10.1073/pnas.1708793114

SI Materials and Methods

Animal Tissues. All experiments with domestic duck (*A. platyrhynchos domesticus*) and chicken (*G. gallus domesticus*) embryos were approved by and performed in accordance with guidelines of Institutional Animal Case and Use Committee of Yale University. Fertilized duck and chicken eggs were purchased from eFowl.com and were used immediately upon arrival or were placed in a cold (13–14 °C) incubator (Wine Enthusiast) for up to 7 d before incubation in an Ova Easy turning incubator (Brinsea) set at 37 °C, 55% humidity, with turning every 90 min until use. Both duck and chicken embryos were killed by rapid decapitation between Hamburger and Hamilton stages 43–45, corresponding to E24–26 in duck and to E19–20 in chicken. Tissues from adult domestic ducks, which were raised and slaughtered for the purpose of human consumption and not for this study, were purchased postmortem at MarWin Farm. Tissues from wild Canada goose (*Branta canadensis*) were gifts from licensed hunters who obtained the birds in North Dakota (Jeffrey Laursen, North Dakota license no. OLN03498597 issued 17 October 2013, Harvest Information Program (Hip) no. 10530354 and Charles Pederson, North Dakota license no. OLN03499483 issued 18 October 2013, Hip no. 10530758). The wild bird tissues are now held under the salvage permit No. 914001 issued by the Connecticut Department of Energy and Environmental Protection to Kristof Zyskowski (Yale University Peabody Museum).

RNA in Situ Hybridization. TG from embryonic and adult birds were processed and developed with alkaline phosphatase-conjugated anti-digoxigenin Fab fragments as described previously (14). Briefly, TGs were dissected and fixed in 4% paraformaldehyde in PBS for 2 h at 4 °C. Cryostat sections (12–15 μm thick) were processed and probed with a digoxigenin-labeled cRNA. Probes were generated by T7/T3 in vitro transcription from transcript fragments amplified from duck TG cDNA, using the following amplification primer pairs (5′–3′):

NTRK1/TrkA: TCATCGAGAACCCGCAGTACTTC; CGATGGCCTCAGTGTTGGAGAG

NTRK2/TrkB: CCTTTTCGCCATCTGGGTTTG; ACTAAGCCAGTGCACACCAG

PIEZO2, *TRPV1*, and *TRPM8* probes were described previously (14) and were each used here for duck, chicken, and goose TG. Signal was developed with alkaline phosphatase-conjugated anti-digoxigenin Fab fragments. Quantification was performed from 7–12 tissue sections with 1,400–3,000 neurons.

Immunohistochemistry. For immunohistochemical experiments, embryonic duckbill skin was peeled and fixed in Nakane fixative, infiltrated in 30% sucrose, and frozen in isopentane and liquid nitrogen. Sections were cut on a Leica CM3050S cryostat at 4 μm and stained with Tuj1 antibodies (MAB1195; 1:200 dilution; R&D Systems) using the VECTASTAIN Peroxidase ABC kit (Vector Laboratories) for immunoperoxidase detection (PK-4000; Vector) following the manufacturer's instructions. For immunofluorescence experiments, fixed bill-skin sections were cut as above and sequentially washed in PBS, 0.05 M ammonium chloride, 0.1% Triton X-100 in PBS, PBS alone, 0.1% (wt/vol) Sudan Black in TBS, Image-IT reagent (Molecular Probes/Life Technologies no. 136933), Tuj1 antibody diluted 1:250 in 0.1% (wt/vol) BSA, and 10% goat serum (Thermo PI-31873) in PBS, 0.1% BSA in PBS, secondary anti-rabbit antibody conjugated with Alexa Fluor 488 (A-11034; Molecular Probes/Life Technologies) diluted 1:200 in 0.1% BSA and 10% goat serum in PBS, 0.1% BSA in PBS, and PBS alone. Sections were stained with DAPI (1:10,000) (Molecular Probes/ Life Technologies D3571), coverslipped with VECTASHIELD medium (Vector Laboratories), and analyzed on a Zeiss Axio Scope A1 microscope.

For whole-mount immunohistochemistry, bill skin from the far lateral edge of the dorsal bill (~2 mm caudal from the bill tip) was dissected under ice-cold PBS (Teknova) and fixed overnight in 4% paraformaldehyde. After fixation, the skin was rinsed 3 × 5 min in PBS, then washed 5 × 1 h in 0.3% Triton X-100 in PBS (PBST) before incubation with mouse monoclonal antibody against β3-III tubulin (Tuj1; MAB1195; R&D Systems) for 3–5 d at 4 °C in blocking solution consisting of 5% normal goat serum (PI-31873; Thermo Fisher), 20% DMSO, and 75% PBST. Tissue was then washed 5 × 1 h in PBST before incubation with Northern Lights 637-conjugated anti-mouse IgG (NL008; R&D Systems) for 2 d. Tissue was washed 5 × 10 min in PBS and then 4 × 1 h in PBST before dehydration in serial dilutions of methanol/PBS, remaining in 100% methanol overnight. Dehydrated tissue was then cleared in a 1:2 mixture of benzyl alcohol (402834; Sigma) and benzyl benzoate (B-6630; Sigma) for 45 min at room temperature before imaging with either a light-sheet microscope (LaVision Biotech, GmbH) or a Leica SP2 confocal microscope. Image analysis was performed using Fiji (ImageJ). The cumulative density of Herbst and Grandry corpuscles in the duck bill was counted in 2.21 ± 0.56-mm sections of dorsal duckbill skin from three animals.

dPiezo2 Cloning. dPiezo2 (KY012733) was cloned into the pMO vector from duck TG cDNA using dPiezo2 forward (5′-ATGGCCACCGAGGTGCTGTG-3′) and reverse (5′-TCAATTAGTTTTTTCCCTAGTCC-3′) primers designed based on Contig4879 and Contig4877, respectively, from the duck transcriptome (70). The protein sequence of Piezo2 that we cloned from duck TG is shown below and was deposited in the GenBank database under the accession number KY012733:

MATEVLCGLTFRLLLPVCLAAACAFRYNGLSFVYLIYLLLIPLFSEPTKTTMKGHTGRLL
KSLCFTSLSFLLLHIIFQITINSLEARKTIEPGFNCSTWEKTLRQIGFESVKGADAGNVI
RLFIPDIGMFIASLTIWLLCRSLVQKPVTEDAAQCNTQFENEEMAVREKLEPDDALMYEE
DLDGEDGGEGEFEETMKLKFLRRIASLASKLREFIGNMITTTGKVVVTILLGSAGMMVPS
LTSAVYFLVFLGLCTWWSFCQVFDPLIFSCLCVLMAIFSAGHIIGLYLYQLQFFQEVVPP
KDFYARLFGVTSLTQTNCSSTWMIIKNQELHWYHHANPILLLVMYYTLATLIRLWLQEPI
QIPDEEEKSDSGEDDKEIACSPIPMTAERRRSLWYASHYTTDERKVLLVTVNGNPSDYHT
IHPTLPLENGPAKADLYSTPQYKWEPSDDMSEKEEEEGEEEEEEVTQEEKEDVKLHALVS
VFQFIMKQSYICALIAMMAWSITYHSWLTFVLLIWSCTLWMIRDRRKYAMLTSPFMVFYA
NLLLTLQYIWSIELKNDELPQVSGFLERKEPGELASKILFTITFWLLLRQHLTEQKALQL
KEATLSEVKVRSEEDEEKEEELQEGEVAEEEEEEEEEEDDDEDEQDIMKVLGKLVMAMFI
KYWIYVCGGMFFFVSFEGRIVMYKIIYMVLFLFCVALYQVHYEWWRKILKYFWMSVVVYT
MLVLIFIYTYQFESFPGLWKNMTGLDESKLEDLGLKRFSVAELFTRIFIPTSFLLACILH
LHYFHDRFLQLTDLKAVTSKQDNTIYSHAKVNGRVYLIINSLKKKLPNQQNELVHQDGSL
PDITMMNLTASSEKEEDKMLKEAGEKRMEEPDGEGGKGRAEKGKEEEEKDDDKEDDDDED
SESEEEETTDLRNKWHLVIDRLTVLFLKFLEYFHKMQVFVWWILELHIIKIVSSYIIWVT
VKEVSLFNFVFLIAWALALPYAQFRPLASSICTVWTCVIIVCKMLYQLASIDPSTFSSNC
TLPGENETKVDIEELKTSILYSGPVDPAEWVGLRKSYPLLVYLRNNLLMLAILAFEVTIY
RHQEYYRCRNNLTVPVTKPIFHDITRAHLDDGLVNCVKYFINYFFYKFGLETCFLLSVNV
IGQRMDFYAMIHAFWLIAVLYRRRRKAIAEIWPKYCCFLACIITFQYFICIGIPPAPCKD
YPWRSGNANFNSNIIKWLYFPDFIVRPNPVFLVYDFMLLLCASLQRQMFEDENKAAVRIM
AGDNVEICMNLEAASFSQHNPVPDFIYCRSYLDMYKVIIFSYLFWFVLTIIFITGTTRIS
IFCMGYLVACFYFLLFGGDLLLKPIRSILRYWDWLIAYNVFVITMKNILSIGACGYIESL
VKNSCWLIQAFSLACTVKGYRIPSSNVDCKLPSGEAGIIWDSICFAFLLLQRRVFMSYYF
LHVVADIKASQILASRGAELFQATIVKAVKARIEEEKKSMDQLKRQMDRIKARQQKYKKG
KERMISMTQESSEGPEIRKVSEEDDEGEADKEKAKGKKKQWWRPWVDHASIVRSGNYYLF
ETDSEEEEEEEKKEEEEPRKKSAFQRAIGKFASAILALPKSIIKLPKTILQYLIKVAKFV
YQAWITDPKTALRQRRKEKKSFQKEQKRRRKGSGDGGTDADYEDSEEEHVKKKSDGPDNI
IKRIFNILKFTWVLFLATLDSFTAWLNSFSREHIDISTVLRIERCMLTREIKKGNVPTRE
SIHMYYQNHMMKLSRESGLDSIDKNPGQASGLQASERMDSLDSAASRDSISSCYTEATML
FSRQSTLDDLDGPDTVPKTSERARPRLRKMQSMDMSSSSADSGSIVSSEPTQVTMLYSRQ
GTTETIEEVEGEHEEEGAHSASRQDEEEVEDYSLGSEGAMLTPDTDVPLYSTVDSNAEAP
PSYSKAVSFEHLPFGSPDDSAGKSLMMVSPDDSRTDRLNDTILPPLTHELTASELLLHKM
FHDEELEESEKFYVGQPRVLLLIYALYNTLVARSEMVCYFVIILNHMISASMITLVLPIL
IFLWAMLSVPRPSKRFWMTAIVYTEVAIVIKYFFQFGFFPWNKFVDYTKDKPYHPPNIIG
IEKKEGYVHYDLVQLLALFFHRSILKCHGLWDEDEKVDSSTNKEDTDDELSLTGGRRDSS
GSLKSVNLAASVESIHVHFPEQQTAIRRKSSSSASQLSHRSSFSSHRSKRGSTSTRNSSQ
KGSSVLSIKQKSKKDLLMEKFREQMIKAKAFTIKKTLQVYVPIRQFFYNLIHPDYSAVTD
VYVLMFLADTVDFIIIVFGFWAFGKHSAAADITSSLSEDQVPGAFLVMVLIQFGTMVVDR
ALYLKKTVMGKVIFQVILVFGIHFWMFFILPGVTERKFSQNTVAQLWYFVKCVYFGLSAY
QIRCGYPTRVLGNFLTKSYNYVNLFLFQGFRLVPFLTELRAVMDWVWTDTTLSLSSWICV
EDIYAHIFILKCWRESEKRYPQPRGQKKKKVVKYGMGGMIIALLIFIVWFPLLFMSLIKS
VAGITNKPLDVSITITLGGYQPIFTMSAQQNQLKSLNQTDFNAFLGSYRGNAAALQFLEG
YGIEDITLADLEGNSNSLWTISPPSREKMIQGLLDFSAEFTVVLSWSIQRNLTLGAKAEI
ASDKLTFGLPVKTRKDIATMMSGKQSEKVTLETVYPYYIKAPSDSLAKPIKQLLTDCRWE
NITVSLVKNVSDEGVREWWVLNQLGKRYKTSEESLELFIFSDKVSPPSLGFLAGYGIMGL
YASVVLVVGKFVREFFSGISHSIMFEELPNVDRILKLCTDIFLVRETGELELEEDLYAKL
IFLYRSPETMIKWTREKTN

Dissociation of Trigeminal Neurons. Embryonic TG were dissected in ice-cold PBS (Teknova), chopped with scissors in HBSS, and dissociated in collagenase (Roche) (1 mg/mL in HBSS) for 15 min at 37 °C, with light agitation half-way through incubation. Neurons were next incubated in 0.25% trypsin-EDTA at 37 °C for 10 min and then were quenched in warm DMEM+ (DMEM with 10% FBS, 1% penicillin/streptomycin, and 2 mM glutamine). Cells were gently triturated using plastic P1000 and P200 pipette tips and were centrifuged for 5 min at 100 × *g* before resuspension. For qPCR and Western blot analysis, cells were diluted with DMEM+ to ∼2 TGs/mL, and 1 mL of cell suspension was plated onto a six-well cell-culture dish. For electrophysiological analysis, 15 μL of cell suspension was plated on Matrigel (BD Bioscience)-coated coverslips in a 12-well cell-culture plate (1:100 in PBS) and placed in a 37 °C cell-culture incubator in 5% CO_2 for 30–45 min before 0.5 mL DMEM+ was added to each well.

siRNA Transfection. Dissociated duck TG neurons were transfected with siRNAs at a final concentration of 350 nM using Lipofectamine 3000 (Thermo Fisher) according to the manufacturer's instructions. Medium was changed 6 h after transfection, and cells were used for qPCR, Western blotting, or electrophysiology 48 h after transfection. Piezo2 siRNA#1 (5′-UAAUGUAAUUGGUCAACGA-3′) was custom-synthesized by Dharmacon with the DY547 fluorophore on the 5′ end of the sense strand and UU overhangs on the 3′ end of sense and anti-sense strands. RNA-induced silencing complex-free siGLO siRNA (D-001600l; Dharmacon) was used as control.

qPCR. Total RNA was extracted from untransfected or siRNA-transfected dissociated duck trigeminal neurons plated onto a six-well plate, using the TRIzol reagent (Invitrogen). The lysates were made from all the cells in the transfection well, including those that did not receive the fluorescent siRNA. One microgram of total RNA was used to synthesize cDNA using the qScript cDNA Supermix (95048; Quanta Biosciences). qPCR calibrations and normalizations were performed using the Illumina Eco System machine in accordance with the manufacturer's instructions. Each reaction was run in triplicate, using duck *Eno2* gene as the reference. Amplification primer pairs (5′–3′) were *Piezo2*: GCAGGAATCATCTGGGACAGT; AGCCTTGACAATTGTAGCCTG (Piezo2 product size 159 bp); *Eno2*: ACCAATGTGGGTGATGAG; TATTTGCCATCCCGGTAG (Eno2 product size 158 bp). Electrophysiological data were included from siRNA transfections where Piezo2 levels in the control group matched those of untransfected cells, and knockdown of Piezo2 was confirmed by qPCR.

Western Blotting. siRNA-transfected dissociated duck trigeminal neurons (three wells of a six-well plate per sample), plasmid-transfected HEK293 cells (one well of a six-well plate per sample), freshly extracted whole duck TG (six TGs per sample), or dorsal bill skin (50 mg per sample) were washed with PBS and lysed by homogenization with a plastic pestle in a 1.5-mL tube in 250 μL of lysis buffer [100 mM NaCl, 20 mM KCl, 10% (vol/vol) glycerol, 1% (wt/vol) CHAPS, 10 mM Hepes/NaOH, pH 7.5], followed by incubation on a nutating platform at 24 rpm for 20 min at 4 °C to solubilize membrane proteins. The lysates were made from all the cells in the transfection well, including those that did not receive the fluorescent siRNA. The detergent-insoluble fraction was pelleted by centrifugation at 14,000 × *g* for 10 min at 4 °C, and the supernatant containing detergent-soluble proteins was collected. Total protein concentration was determined by the Bradford assay. Bill skin lysates were mixed 1:3 (vol/vol) with buffer [Nonidet P-40 containing 150 mM NaCl, 1 mM EDTA, 1% (wt/vol) Nonidet P-40, 25 mM Tris/HCl, pH 7.4] and were incubated on a nutating platform at 24 rpm for 2 h at room temperature. Treatment with Nonidet P-40 buffer facilitated the detection of Piezo2 in skin lysates but had no effect on lysates from TG. Lysates containing 1–100 μg of total protein were treated with a Laemmli sample buffer containing 2% (wt/vol) SDS (final concentration) for 7 min at 50 °C, separated on a 4–15% polyacrylamide gel, and blotted onto a PVDF membrane. The membrane was blocked in Tris-buffered saline with 3% nonfat milk and 1% Tween 20 for 1 h at room temperature and was incubated overnight at 4 °C with monoclonal antibodies against chicken actin (ACTN05 C4, ab3280; 1:1,000 dilution; Abcam) or custom affinity-purified rabbit polyclonal antibody against Piezo2 (57-1; 1:250 dilution; Abcam) raised against the VPKTSERARPRLRKM peptide corresponding to amino acids 1,816–1,830 in dPiezo2 (KY012733) and amino acids 1,791–1,805 in mPiezo2 (Q8CD54-1). Following incubation with peroxidase-conjugated secondary antibodies, blots were developed using the West Pico or West Femto chemiluminescent substrate (Thermo Fisher) and were detected on an X-ray film. To measure the effect of siRNA treatment on Piezo2 expression, six duck TGs were dissociated as described above, divided into two pools, and transfected with control or Piezo2 siRNA using three independent reactions for each condition on a six-well plate. Forty-eight hours later, cells from each three-well set were combined, lysed, and immunoblotted for Piezo2 and actin as described above. The Piezo2 signal was normalized to actin and presented as average from three independent TG preparations.

Patch-Clamp Electrophysiology. HEK293T cells were used because of their low background MA current (34). The cells were cultured in DMEM+. The cells were not authenticated or tested for mycoplasma contamination. Plasmids encoding mPiezo2 (pCMV-Sport6-mPiezo2, a gift from Ardem Patapoutian, The Scripps Research Institute, San Diego) (34) and dPiezo2 (pMO-dPiezo2)

were cotransfected with the pMO-GFP plasmid in a 10:1 ratio using Lipofectamine 2000 (Thermo Fisher) according to the manufacturer's instructions. Briefly, DNA–Lipofectamine complexes were formed during incubation in Opti-MEM (Gibco) for 20 min at room temperature before being added to HEK293T cells cultured to 70–80% confluence in six-well plates. The medium was changed 6 h after transfection. Cells were plated on Matrigel (diluted 1:100 in PBS)-coated coverslips 18–24 h after transfection and were recorded within 48–60 h after plating. The internal solution for recording from Piezo2 in HEK293T cells consisted of (in mM): 133 CsCl, 5 EGTA, 1 $CaCl_2$, 1 $MgCl_2$, 10 Hepes, 4 Mg-ATP, 0.4 Na_2-GTP, pH to 7.3 with CsOH. The external solution contained the following (in mM): 140 NaCl, 5 KCl, 10 Hepes, 2.5 $CaCl_2$, 1 $MgCl_2$, 10 glucose (pH 7.4 with NaOH).

HEK293T cell electrophysiology was acquired on an Olympus BX51-WI microscope with an Orca flash2.8 camera (Hamamatsu), a MultiClamp 700B patch-clamp amplifier, and a Digidata 1550 digitizer (Molecular Devices). Recordings were acquired using pCLAMP software (Molecular Devices) sampled at 20 kHz and low-pass filtered at 2–10 kHz. Mechanical stimulation was performed using a blunt glass probe (2–4 μm at the tip) mounted on a preloaded Piezo actuator stack (Physik Instrumente GmbH), with the angle of the mechanical stimulation probe set to 32° from the horizontal plane. Membrane potential was clamped at −80 mV. HEK293T cell measurements were not corrected for the liquid junction potential (15.2 mV). For mechanical stimulation experiments, cells were stimulated within 5 min of establishing whole-cell recording. After breaking into the cell, the stimulation probe was positioned under visual guidance so that it just touched the cell membrane, at a location generally opposite the patch pipette. The probe was then moved toward the cell in 1-μm increments at a velocity of 800 μm/s, held in position for 150 ms, then retracted at the same velocity. This stimulation was performed until either the peak amplitude of the evoked current reached a saturating value for multiple sweeps or recording was lost or the cell died. Electrophysiology data were converted from pCLAMP format using TaroTools and then were analyzed using custom routines in Igor Pro-6.3 (WaveMetrics). Statistical analysis was also performed using Prism (GraphPad).

Voltage-clamp recordings from dissociated duck and chicken trigeminal neurons were performed using the procedures, solutions, and mechanical stimulation protocols previously described (14). Recording and mechanical stimulation conditions were identical to those described above for HEK293T cells, except that neurons were clamped at −60 mV (−74.6 mV after liquid junction potential correction). The internal solution consisted of (in mM) 130 K-methanesulfonate, 20 KCl, 1 $MgCl_2$, 10 Hepes, 3 Na_2ATP, 0.06 Na_3GTP, 0.2 EGTA, pH 7.3 with KOH (final [K+] = 150.5 mM). The external solution contained the following (in mM): 140 NaCl, 5 KCl, 10 Hepes, 2.5 $CaCl_2$, 1 $MgCl_2$, 10 glucose (pH 7.4 with NaOH). The liquid junction potential was 14.6 mV and was subtracted offline. Patch pipettes of borosilicate glass with an o.d. of 1.5 mm (Warner Instruments no. G150F-3) were pulled to a tip resistance of 1.5–5 MΩ using a P-1000 puller (Sutter Instruments). Immediately after whole-cell recording was established, resting potential was measured in I = 0 mode. Half the mechano-stimulation electrophysiology data were acquired on the equipment described above, and the other half were acquired on a Zeiss Axio-Examiner with an Orca flash 4.0 camera (Hamamatsu) and an Axopatch 200-B amplifier/Digidata 1440 (Molecular Devices), as previously described (14). The angle of the mechanical stimulation probe was set to either 32° or 55° from the horizontal plane. There was no statistical effect of angle on datasets acquired on both rigs. To quantify the inactivation rate constant, the decaying phase of the MA current was fit to the single exponential equation $I = \Delta I^{*}\exp\hat{}(-t/\tau_{inact})$, where ΔI is the absolute change in current (pA) from baseline to peak, t is the time span in seconds for the curve fit from peak to plateau, and τ_{inact} is the inactivation rate constant, as described elsewhere (14). Cells with series resistance >20 MΩ were not included in voltage-clamp analysis of MA current tau or amplitude but were used in quantifications of the percentage of neurons responding to mechanical stimulation.

Ex Vivo Electrophysiology. Following rapid decapitation, the brain and ipsilateral eye were removed under ice-cold oxygenated artificial cerebrospinal fluid (ACSF) containing (in mM): 130 NaCl, 3.5 KCl, 24 $NaHCO_3$, 1.25 NaH_2PO_4, 1.2 $MgCl_2$, 1.2 $CaCl_2$, and 10 dextrose. The solution was bubbled with 95% O2/5% CO_2 (pH 7.4, osmolarity 300–310 mOsm). Skull and membranes covering the TG surface were gently removed to expose the TG. The head was then pinned to the Sylgard (Dow-Corning)-coated floor of a custom chamber. The recording chamber was transferred to the stage of an Olympus BX51WI microscope where cells were visualized using custom optics previously described (71). Then 0.2–0.3 mL collagenase (1 mg/mL) in ACSF was applied by stopping perfusion of ACSF for 5 min and gently dripping collagenase through an 18-G syringe directed toward the exposed surface of the TG. If necessary, this procedure was repeated. Otherwise, the preparation was continuously perfused with oxygenated ACSF at room temperature (1–2 mL/min) for the duration of the recording. Extracellular suction recordings were performed under visual control by pulling the soma into a polished glass pipette (front-filled with ACSF from the recording chamber) with an ∼15-μm tip diameter. We did not observe spontaneous spiking during these manipulations. Once a recording was established, the dorsal bill was lightly swept with a no. 2 round paint brush (Winsor and Newton) to determine the location of the neuron's receptive field. Neurons with receptive fields in the dorsal bill were mechanically stimulated using either (*i*) a stimulus probe consisting of a 200-μm-diameter stainless-steel rod with a blunt end mounted on a manual manipulator (Narshige) or (*ii*) the lever arm of a 300B mechanical stimulator (Aurora Scientific) holding a probe with a 2-mm rounded metal tip. For (*i*), stimulus onset and offset were recorded by manual tagging in pCLAMP. Neurons were capable of responding to the application or removal of forces as low as 7 mN and deflections of less than 0.5 μm. In all cases neurons were rapidly adapting. Neurons were most likely to respond to initial touch or rapid gentle brushing rather than to increases of force from a static basal force. Receptive fields were <1 mm in diameter.

Quantification and Statistical Analysis. Statistical parameters and significance are reported in the figures and figure legends. Data are expressed as means ± SE or SD unless stated otherwise in figure legends and were analyzed using Igor Pro-6.3 (WaveMetrics), Prism (GraphPad), or MATLAB (MathWorks). All biological data were obtained from samples of at least two animals. Piezo2 siRNA experiments were included in the dataset when the amplitude and number of cells with MA current in the control siRNA group did not statistically differ from untransfected neurons. Sample size and statistical tests are reported in figure legends, were determined based on our own previous experience with these assays and published data (64, 66), and were chosen to maximize statistical significance. Statistical tests were chosen based on normality of distributions and variance equality or lack thereof.

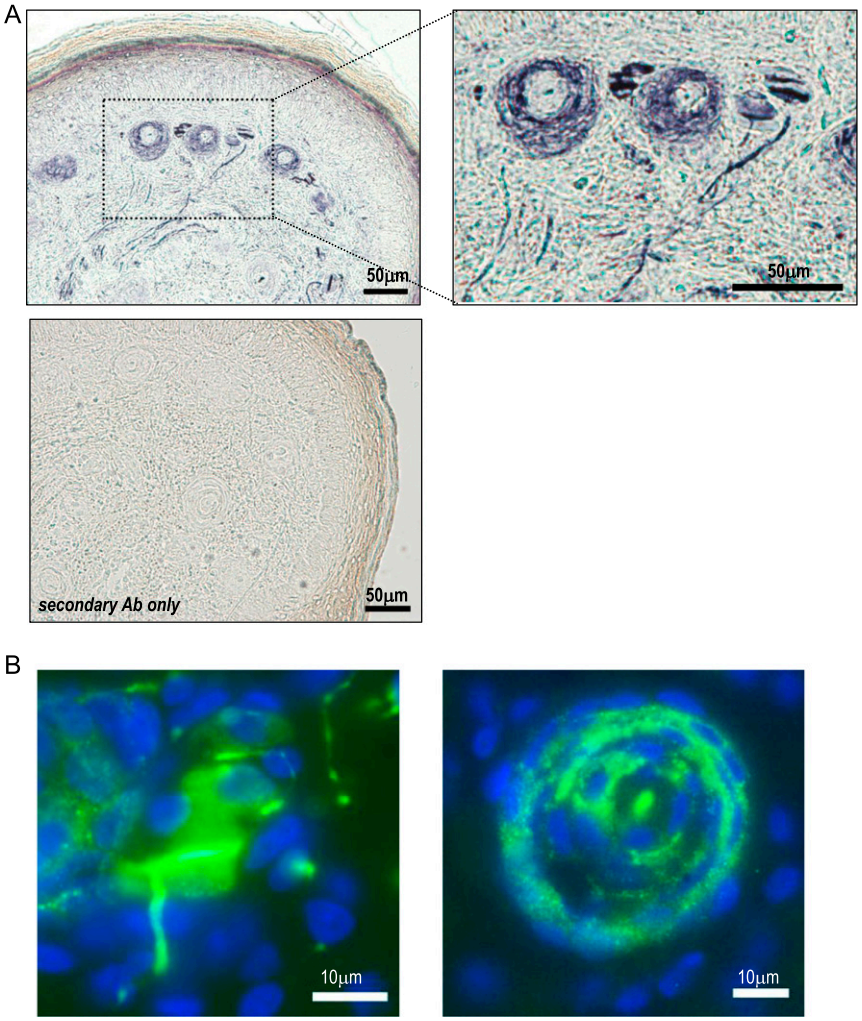

Fig. S1. (*A*) Symbol-free images from Fig. 1*A* (*Upper*) and a control staining of dorsal duckbill skin with secondary antibody only (*Lower*). (*B*) Symbol-free images from Fig. 1 *B* and *C*.

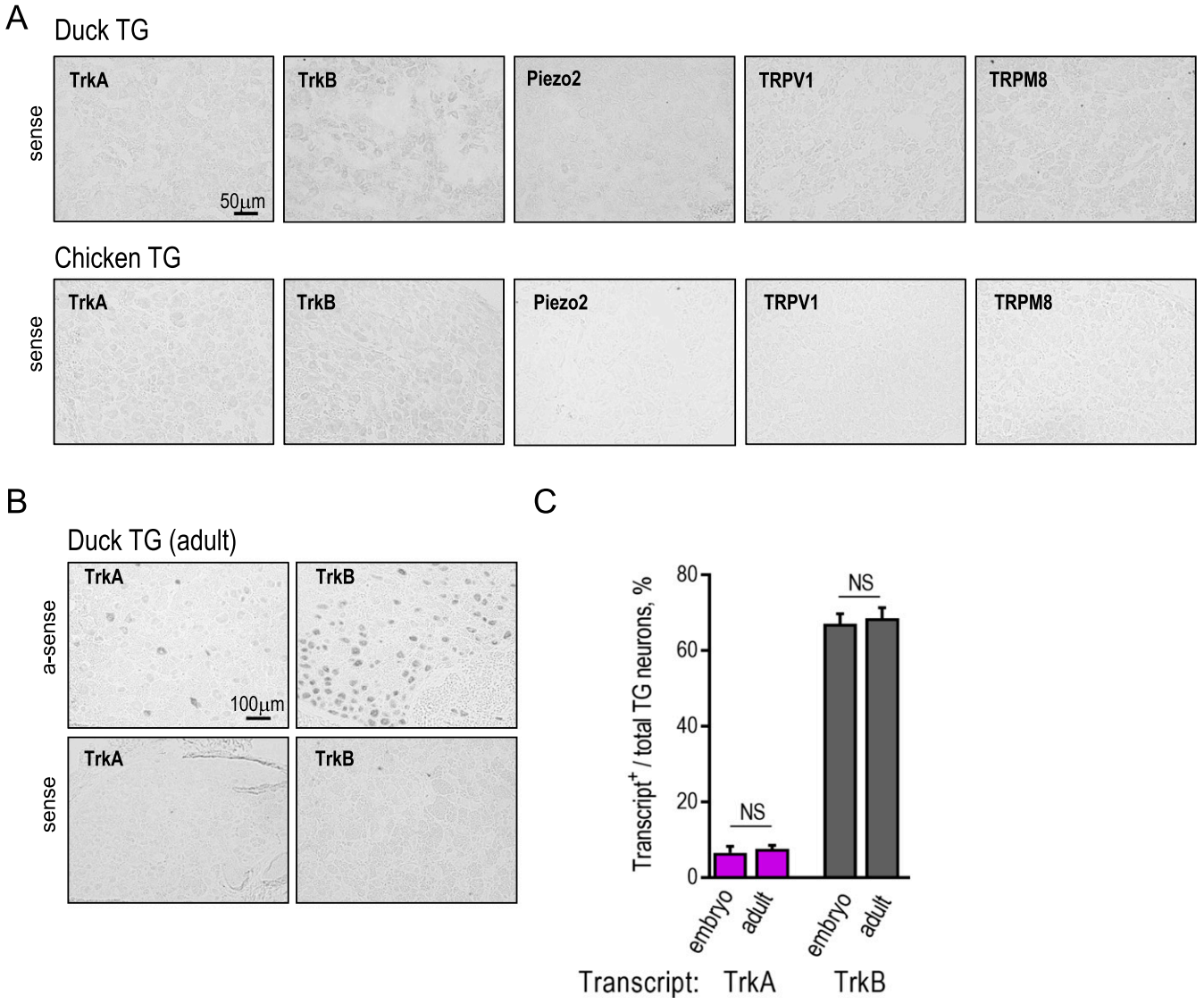

Fig. S2. (*A*) Representative images of control (sense) RNA in situ hybridization for the indicated targets in late-embryonic duck and chicken trigeminal neurons. (*B*) Exemplar images of RNA in situ hybridization. (*C*) Quantification of the abundance of neurons expressing the indicated targets in late-embryonic and adult duck TG (mean ± SE from ≥1,804 neurons from at least 10 TG sections from at least two animals for each target; NS, not significant, $P > 0.05$, two-tailed *t* test).

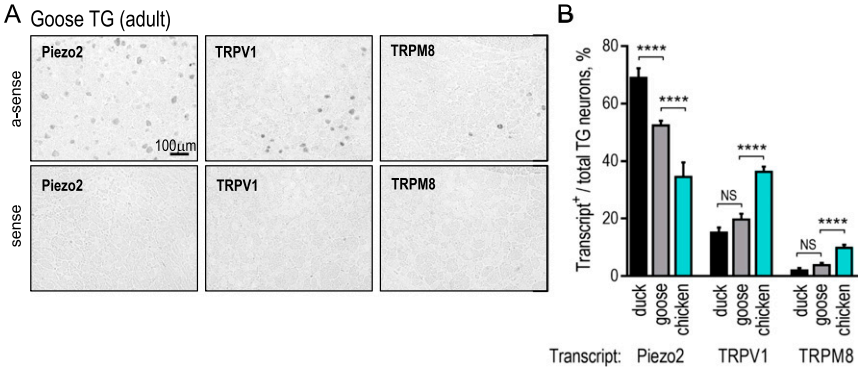

Fig. S3. (*A*) Representative images of RNA in situ hybridization for the indicated targets in adult goose trigeminal neurons. (*B*) Quantification of the abundance of neurons expressing the indicated targets in duck, chicken, and goose TG based on RNA in situ hybridization analysis (mean ± SE from ≥1,700 neurons obtained from at least seven TG sections from at least two animals for each target; ****$P \leq 0.0001$; NS, not significant, $P > 0.05$; two-tailed *t* test.). Duck and chicken data are as in Fig. 2*B*.

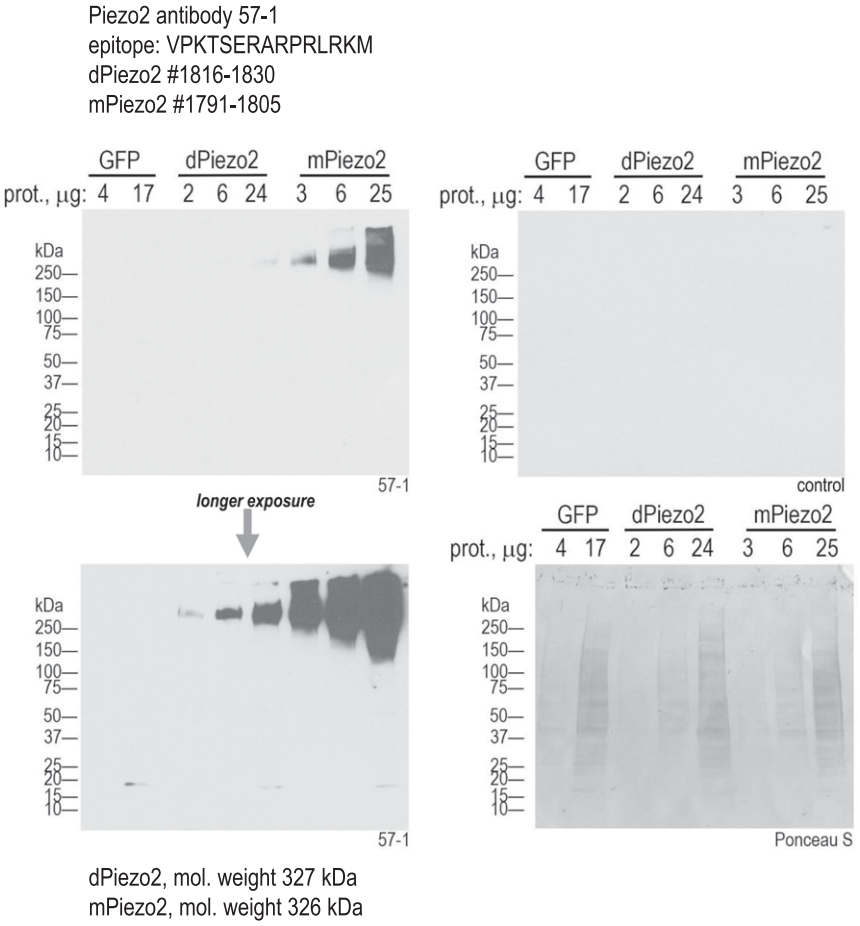

Fig. S4. Validation of Piezo2 antibody by immunoblotting. Piezo2 detection by Western blotting in lysates of HEK293T cells expressing the indicated constructs from a pMO (GFP, dPiezo2) or pCMV-Sport6 (mPiezo2) plasmid, using anti-Piezo2 antibody raised against the indicated conserved epitope in dPiezo2 and mPiezo2 (antibody 57-1) or secondary antibody only (control).

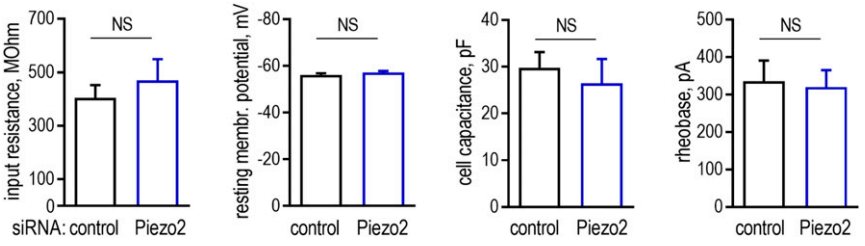

Fig. S5. Quantification of the effect of control or Piezo2 siRNA on functional parameters of duck TG neurons. Resting membrane potential values were not corrected for liquid junction potential. Data are shown as mean ± SE from 67 (control siRNA) and 51 (Piezo2 siRNA) neurons. (NS, not significant, $P > 0.05$, nonparametric Mann–Whitney *U* test.)

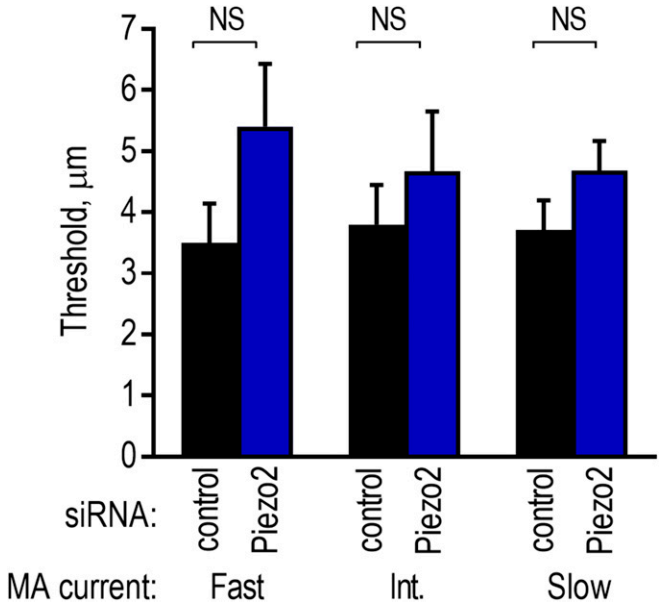

Fig. S6. Quantification of MA current activation threshold in control and Piezo2 siRNA-treated duck TG neurons (mean ± SE from 67 control siRNA and 51 Piezo2 siRNA neurons; NS, not significant, $P > 0.05$, one-way ANOVA with Bonferroni correction for multiple comparisons).

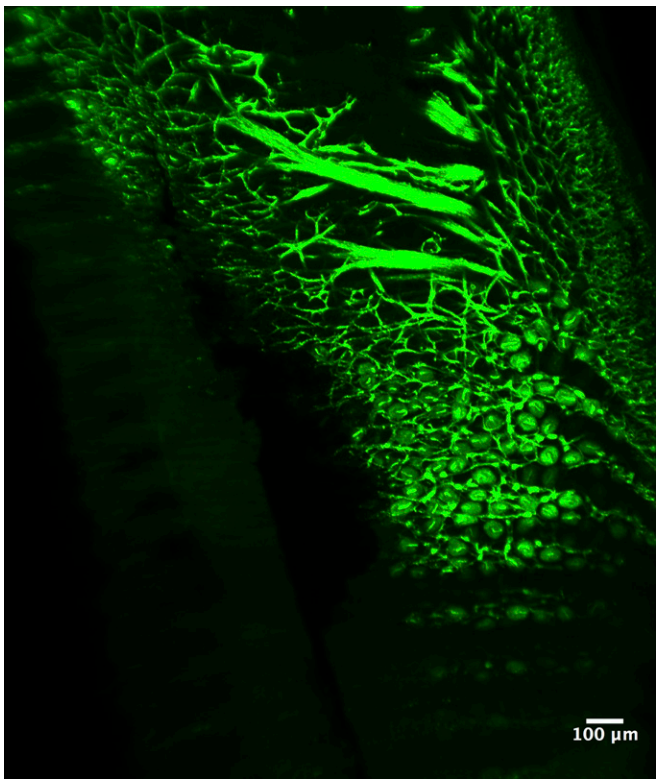

Movie S1. Light-sheet microscopy of a whole-mount preparation of a patch of dorsal bill skin (0.64 mm^2) from a late-stage duck embryo stained with Tuj1 antibody. Staining reveals a high-density population of Grandry and Herbst mechanosensory corpuscles together with underlying trigeminal mechanoreceptors.

Movie S1